THE JOURNAL OF PHYSICAL CHEMISTRY B
A JOURNAL OF THE AMERICAN CHEMICAL SOCIETY

pubs.acs.org/JPCB Article

Cleavage-Resistant Protein Labeling With Hydrophilic Trityl Enables Distance Measurements *In-Cell*

Zikri Hasanbasri, Kevin Singewald, Teresa D. Gluth, Benoit Driesschaert,* and Sunil Saxena*

Cite This: https://doi.org/10.1021/acs.jpcb.1c02371 Read Online

ACCESS | Metrics & More | Article Recommendations | Supporting Information

ABSTRACT: Sensitive *in-cell* distance measurements in proteins using pulsed-electron spin resonance (ESR) require reduction-resistant and cleavage-resistant spin labels. Among the reduction-resistant moieties, the hydrophilic trityl core known as OX063 is promising due to its long phase-memory relaxation time (T_m). This property leads to a sufficiently intense ESR signal for reliable distance measurements. Furthermore, the T_m of OX063 remains sufficiently long at higher temperatures, opening the possibility for measurements at temperatures above 50 K. In this work, we synthesized deuterated OX063 with a maleimide linker (mOX063-d_{24}). We show that the combination of the hydrophilicity of the label and the maleimide linker enables high protein labeling that is cleavage-resistant *in-cells*. Distance measurements performed at 150 K using this label are more sensitive than the measurements at 80 K. The sensitivity gain is due to the significantly short longitudinal relaxation time (T_1) at higher temperatures, which enables more data collection per unit of time. In addition to *in vitro* experiments, we perform distance measurements in *Xenopus laevis* oocytes. Interestingly, the T_m of mOX063-d_{24} is sufficiently long even in the crowded environment of the cell, leading to signals of appreciable intensity. Overall, mOX063-d_{24} provides highly sensitive distance measurements both *in vitro* and *in-cells*.

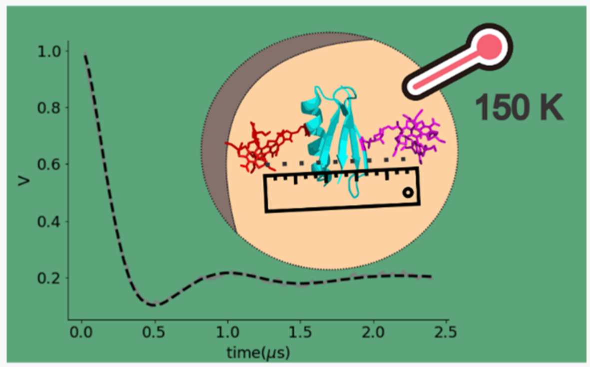

■ INTRODUCTION

Understanding how proteins adapt in their cellular environments is of immense interest in structural biology. The crowded environment inside cells can affect protein folding and stability.[1−7] For example, phosphoglycerate kinase (PGK) is more stable in zebrafish tissues[8] and human osteosarcoma cells[5] than *in vitro*. The increase in stability due to molecular crowding has also been observed with other proteins such as frataxin,[9] ubiquitin,[10] hen egg white lysozyme,[11] and calcineurin.[12] In contrast, the dimerization of the baculoviral IAP repeat domain of X-chromosome-linked inhibitor of apoptosis is destabilized *in vivo*.[13] The destabilization effects are also seen in other protein dimers that are not spherical in shape.[14,15] These experiments are indicators that the *in-cell* environment modulates protein structure and function, which vary case-by-case. Overall, *in-cell* experiments are required to understand the behavior of proteins in the context of cellular function.

In this context, ESR has emerged as a widely applicable technique to measure dynamics and distance constraints *in vitro* and *in-cell*. For such ESR measurements, the normally diamagnetic proteins can be functionalized with a spin label using site-directed spin-labeling methodologies.[16−19] The combination of ESR and spin labeling enables the measurement of the dynamics at the labeled site[20,21] and the measurement of distances between the labeled sites of a protein.[22−28] Distance measurements have been particularly useful for shedding light on the changes in protein conformations,[29−37] the assembly of large complexes,[38−41] and the binding of substrates and metal ions.[42−45] Additionally, these distance measurements have been performed *in-cell* for proteins[46−48] and DNA.[49,50] The primary challenge for distance measurements *in-cell* is the reduction of spin labels within the highly reducing cytosolic environment.[51] An intriguing new strategy for *in-cell* measurements is the use of genetically encoded noncanonical amino acid technology as an *in situ* labeling strategy.[52−55] In particular, a photocaged radical amino acid can be incorporated into a protein during translation.[56] Only after the induction of light will the photocage be released to expose the nitroxide radical for ESR measurements. In addition to noncanonical amino acids, reduction-resistant spin labels such as sterically shielded nitroxides,[57,58] Gd(III)-based spin labels,[59−61] and triarylmethyls (TAMs, trityls)[62−64] have been developed.

Trityls have a lot of potential as a class of spin labels for several reasons. First, trityls are highly resistant to reduction *in*-

Received: March 16, 2021
Revised: April 29, 2021

https://doi.org/10.1021/acs.jpcb.1c02371
J. Phys. Chem. B XXXX, XXX, XXX−XXX

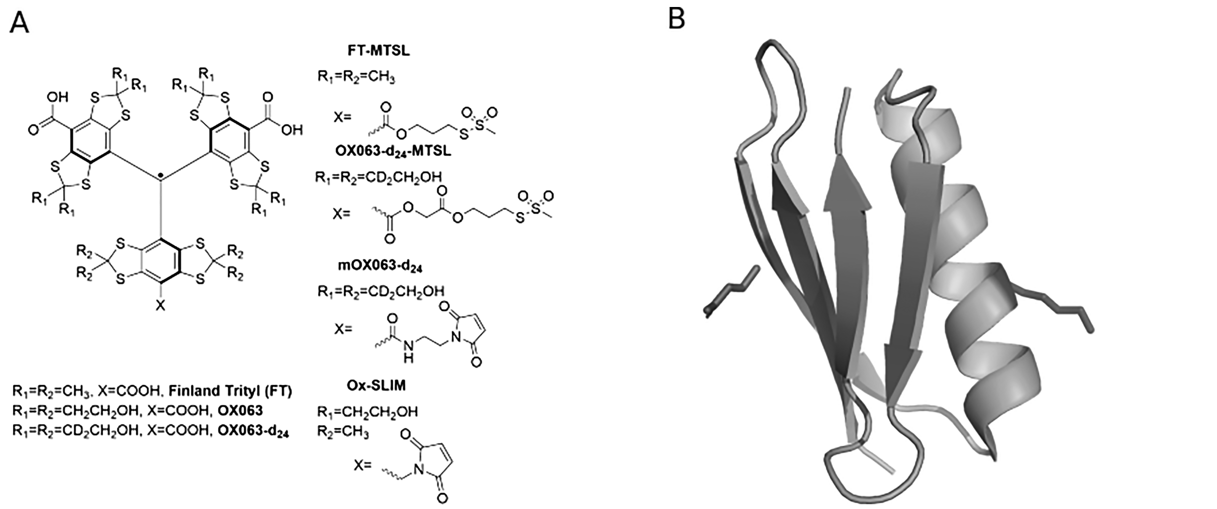

Figure 1. (A) Representation of trityl-based spin labels, FT-MTSL, OX063-d_{24}-MTSL, mOX063-d_{24}, and Ox-SLIM. (B) Three-dimensional model of E15C/K28C GB1 based on the wild-type GB1 crystal structure (PDB:2QMT). The side chains of the mutated cysteines are represented as lines.

cell due to the steric shielding of its radical.[65−67] Second, trityls have appreciable relaxation times even at physiological temperatures.[68] Third, trityls have a narrow spectral shape that leads to efficient excitation of the electrons and intense ESR signal.[69] Overall, trityl spin labels have proved suitable for distance measurements at physiological temperatures or *in-cell*. The most explored trityl spin labels are based on the Finland trityl radical (FT) shown in Figure 1A, which have successfully provided distance measurements at room temperature[70,71] and *in-cell*.[72,7372,73] However, FT-based spin label usage is still challenging due to the complications in the labeling process.

The spin-labeling process typically entails a reaction between the spin label and a cysteine residue to label the protein at a specific site. However, FT can bind nonspecifically to membranes[74] or proteins.[75] Additionally, FT tends to self-aggregate.[76,77] As a result, efficient labeling of FT requires extensive washing of proteins that are immobilized on a solid support[63] or maintaining FT concentration to be less than 30 μM throughout the process to minimize aggregation.[78]

Even after the labeling process, the phase-memory relaxation time (T_m) of FT is significantly reduced upon protein binding,[63,78] which leads to a weaker signal. Additionally, the longitudinal relaxation time (T_1) is significantly long at temperatures that are typical for ESR distance measurements ($\leq$50 K),[78] which leads to longer experimental time. Overall, the short T_m and long T_1 of FT-based spin labels diminish the sensitivity gain from the efficient excitation of FT. As a result, FT's sensitivity for distance measurements is comparable to distance measurements using commercially available nitroxide spin label.[78]

As an alternative, a hydrophilic trityl spin label, based on the OX063 radical shown in Figure 1A, has been recently developed that allows for a straightforward labeling procedure without nonspecific binding or aggregation.[79] Interestingly, deuterated OX063 (OX063-d_{24}) was reported to have the longest transversal relaxation time at 50 K to date (T_m = 6.3 μs).[79] Additionally, OX063-d_{24} has been shown to also have a sufficiently long phase-memory relaxation time even at 200 K (T_m = 3 μs).[46] Because T_1 is generally shorter at higher temperatures, OX063-d_{24} has the potential for highly sensitive distance measurements at temperatures higher than 50 K. Despite OX063-d_{24}'s improvement over FT, OX063-d_{24} only utilized a methanethiosulfonate linker so far, which is a limiting factor for *in-cell* experiments. This linker labels a protein by forming disulfide bonds with cysteines, which can be cleaved inside cells.[48] On the other hand, a maleimide linker reacts with a cysteine to form a thioether bond, which is uncleavable under normal physiological conditions.[47] In response to the need of a hydrophilic trityl with an uncleavable linker, a hybrid of OX063 and short-linker maleimide (SLIM)[73] known as Ox-SLIM was recently developed (Figure 1A).[80] Unlike OX063, the trityl core of Ox-SLIM has one of its bisthioketalaryl moieties remain unhydroxylated to bear the short maleimide linker. The hydrophilicity of Ox-SLIM permitted the labeling efficiency of ~85%. These results motivate the development of hydrophilic trityl labels with high labeling efficiency for *in-cell* distance measurements.

To increase the viability of OX063-d_{24}-based spin labels, we have developed a new OX063-d_{24} spin label with a maleimide linker (mOX063-d_{24}), as shown in Figure 1A. The maleimide linker allows for mOX063-d_{24} to maintain its linkage with the protein *in-cell*.[81] We explored two aspects of mOX063-d_{24} for distance measurements in proteins. First, we show how mOX063-d_{24} provides highly sensitive distance measurements at temperatures higher than the typical $\leq$50 K *in vitro*. Second, we showcase the usage of mOX063-d_{24} for experiments *in-cell*, specifically in *Xenopus laevis* oocytes. When exploring these two aspects, spin labeling and distance measurements were done on the immunoglobulin binding domain of protein G (GB1),[82] a 56-residue globular protein (Figure 1B).

■ METHODS

Synthesis of mOX063-d_{24}. OX063-d_{24} trisodium salt (112 mg, 0.077 mmol, 1 equiv), synthesized using our previously reported protocols,[83] was dissolved in anhydrous dimethylformamide (DMF) (100 mL) under an argon atmosphere at room temperature. Benzotriazol-1-yl-oxytripyrrolidinophosphonium hexafluorophosphate (PyBOP) (28 mg, 0.054 mmol, 0.7 equiv) in DMF (1 mL) was added; the green solution turned into a red-brown colored solution. Then, *N*-(2-aminoethyl)maleimide trifluoroacetate salt (23 mg, 0.09 mmol, 1.2 equiv) in DMF (1 mL) and *N*,*N*-diisopropylethylamine (DIEA) (26.8 μL, 1.4 mmol, 2 equiv) were added. The solution turned back to green. The reaction mixture was

Scheme 1. Synthesis of mOx063-d_{24} from Ox063-d_{24}

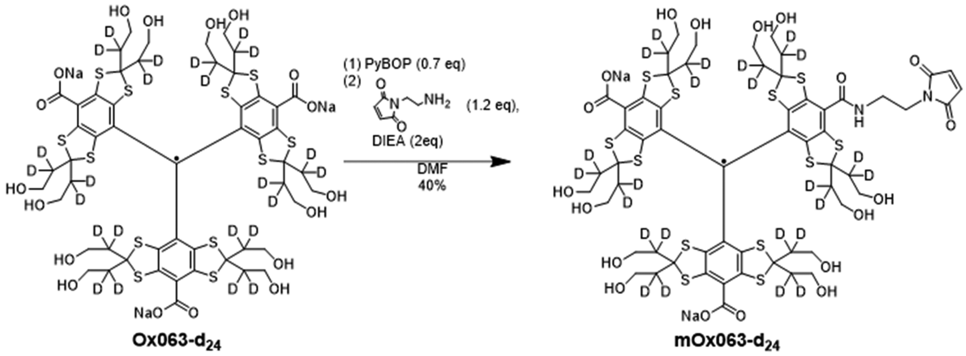

diluted 20× with deionized water and acidified to approximately pH~2 with trifluoroacetic acid (TFA). The crude product was loaded into a C18 cartridge and purified by reverse-phase chromatography using a C18 column with a gradient of water/acetonitrile (both containing 0.1% TFA) 95/5 to 85/15. The purified product was freeze-dried, dissolved in water, titrated to pH = 7 with NaOH, and freeze-dried again to provide 48 mg (40%) of mOX063-d_{24} as a disodium salt. The purity assessed by high-performance liquid chromatography (HPLC) reached >95%, as shown in Figure S1. HRMS characterization is shown in Figure S2.

GB1 Labeling Protocol. E15C/K28C GB1 expression and purification were performed, as previously described.[84] The GB1 mutant was reacted with tris(2-carboxyethyl)phosphine (TCEP) overnight at 4 °C to reduce any disulfide formation. To label the protein, GB1 was run through four 5 mL GE Healthcare Hitrap desalting columns, to remove any TCEP, directly into a solution of mOX063-d_{24}. The final solution of 10:1 of mOX063-d_{24}/GB1 was allowed to react overnight at 4 °C. The spin-labeled protein was concentrated using Sartorius VivaSpin Turbo 4 centrifugal filter units with a molecular weight cutoff of 5 kDa to remove the unreacted label. The final solution was prepared in PBS, pH 7.4. Concentration and labeling efficiencies were calculated from UV−vis measurement using a Nanodrop2000 Spectrophotometer from Thermo Scientific. The extinction coefficient of GB1 was obtained from the ProtParam tool (https://web.expasy.org/protparam/). Masses were measured by liquid chromatography electrospray ionization time-of-flight mass spectrometry (LC-ESI-TOF-MS, Bruker Micro TOF, Billerica, MA).

Cellular Extracts and Oocyte Microinjection. Oocytes were obtained from Carolina Biological Supplies. The cytosol was extracted following the previously published protocol.[85] The cytosol sample was prepared at 50 μL containing doubly labeled mOX063-d_{24}-GB1 (200 μM spin concentration) and drawn into Pyrex capillary tubes (I.D. = 0.8 mm) for room-temperature continuous-wave (CW) ESR experiments. For *in-cell* pulsed-ESR experiments, 50 nL of doubly labeled mOX063-d_{24}-GB1 (2 mM spin concentration) was microinjected into 12 oocytes following the previously published protocol.[85] The microinjected oocytes were inserted into a Quartz Q-band sample tube (2 mm I.D. and 3 mm O.D.) and incubated at room temperature for 30 min before being flash-frozen in liquified methylacetylene-propadiene propane (MAPP) gas. The Q-band *in-cell* sample was estimated to be 60 μL of ~20 μM bulk spin concentration.

ESR Measurements. Room-temperature continuous-wave (CW)-ESR experiments were performed on a Bruker ElexSys E680 CW/FT X-band spectrometer using a Bruker ER4122 SHQE−W1 high-resolution resonator. CW ESR samples were prepared in Pyrex capillary sample tubes. CW ESR experiments were run at a center field of 3520 G with a sweep width of 20 G, microwave frequency of ~9.87 GHz, modulation amplitude of 0.07 G or 0.005 G, and modulation frequency of 100 or 300 kHz[83] for a total of 1024 or 2048 data points using a conversion time of 30.01 ms.

All pulsed experiments were performed on a Bruker ElexSys E680 CW/FT X-band spectrometer equipped with a Bruker ER5106-QT2 resonator for Q-band and a 300 W amplifier. The temperature was controlled using an Oxford ITC503 temperature controller and an Oxford CF935 dynamic continuous-flow cryostat connected to an Oxford LLT 650 low-loss transfer tube. Echo decay experiments used a two-pulse sequence, $\pi/2$-t-π, where t was increased by a step size of 8 ns for 1024 points. T_m values were obtained by fitting the Echo decay results with a stretched exponential decay. The time point where the signal is $1/e$ of the original intensity is the reported T_m value. Inversion recovery experiments followed a three-pulse sequence, π-T_1-$\pi/2$-T_2-π, where T_2 was 400 ns and T_1 was increased by a step size of 1 or 10 μs for 1024 points. The fitting of inversion recovery data is detailed in the Supporting Information. Double quantum coherence (DQC)[22,86] was performed at the field with the maximum signal intensity of mOX063-d_{24}. The DQC experiments followed a six-pulse sequence, $\pi/2$-t_p-π-t_p-$\pi/2$-t_1-π-t_1-$\pi/2$-t_2-π, where t_p and t_2 were increased and decreased, respectively, by 10 ns for 136 points. The initial parameters were set as t_p = 1.3 μs, t_1 = 50 ns, and t_2 = 1.5 μs. To remove the unwanted echo signal, the 64-step phase cycle was implemented.[22,23] The DQC time traces were then analyzed using DeerAnalysis[87] by Tikhonov regularization.

SNR was calculated from the raw DQC time traces using the previously published method.[88] In summary, the raw DQC time trace was fitted to a 5th-order polynomial. The fit was subtracted from the time trace to isolate the noise of the time trace. The noise was used by the software SnrCalculator to calculate the final SNR.

■ RESULTS AND DISCUSSION

Our recent report of the synthesis of the OX063 triarylmethyl radical and its deuterated analogues OX063-d_{24}[83] enables the synthesis of OX063 derivatives such as spin labels. A short maleimide linker was conjugated to OX063-d_{24} using the PyBOP peptide coupling reagent, as depicted in Scheme 1.

https://doi.org/10.1021/acs.jpcb.1c02371
J. Phys. Chem. B XXXX, XXX, XXX−XXX

The mOX063-d_{24} was isolated in 40% yield after purification on C18 alongside with 10% of the dimaleimide derivative.

We overexpressed and labeled E15C/K28C GB1 with mOX063-d_{24} through a reaction between cysteine residues and the maleimide linker. The labeling reaction occurred by incubating E15C/K28C GB1 and mOX063-d_{24} in PBS, pH 7.4, overnight. The solution was filtered through a centrifugal filter with a molecular weight cutoff of 5 kDa to remove free mOX063-d_{24}. We first performed ESI-MS to confirm the covalent attachment of mOX063-d_{24} to E15C/K28C GB1. The data is shown in Figure S3. The MS showed peaks corresponding to doubly labeled, singly labeled, and non-labeled E15C/K28C GB1. This result is expected because of the detachment of the spin label during sample preparation in acidic conditions (trifluroacetic acid) for ESI-MS and has been reported before using a maleimide-linked FT.[78]

The final product was characterized using UV−vis spectroscopy to assess spin-labeling efficiency. This data is shown in Figure 2. The spectrum features two distinctive peaks at 280 and 469 nm. Only mOX063-d_{24} contributes toward the 469 nm peak,[89] while both mOX063-d_{24} and GB1 contribute toward the 280 nm peak. The UV−vis spectrum was analyzed using the deconvolution method, as depicted in Figure 2,[78] which fits the mOX063-d_{24}-GB1 spectrum using GB1's UV−vis spectrum (dash-dotted line) and mOX063-d_{24}'s UV−vis spectrum (dotted line). The deconvolution allowed us to obtain the absorbance of GB1 at 280 nm (ε_{280} = 9970 M^{-1} cm^{-1}) and mOX063-d_{24} at 469 nm (ε_{469} = 16 000 M^{-1} cm^{-1}),[89] which were used to calculate their concentrations. The final concentrations of GB1 and mOX063-d_{24} in the sample are 82.0 and 161.8 μM, respectively. Therefore, the ratio of GB1:mOX063-d_{24} purified is about 1:1.97. Overall, our UV−vis results indicate efficient mOX063-d_{24} labeling of cysteines on GB1.

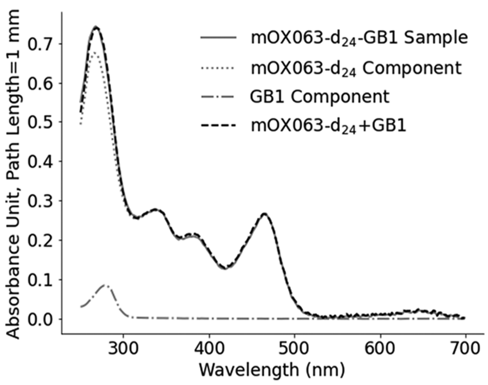

Figure 2. UV−vis spectrum of the mOX063-d_{24}-GB1 sample (gray line). The mOX063-d_{24}-GB1 spectrum was deconvoluted into its GB1 (dash-dotted line) and mOX063-d_{24} (dotted line) components. The sum of the two components (dashed line) fits well with the mOX063-d_{24}-GB1 spectrum.

To further validate the labeling efficiency, the mOX063-d_{24}-GB1 sample was characterized using CW−ESR at room temperature. Figure 3A,B shows the CW−ESR spectrum of mOX063-d_{24} bound to GB1 and free mOX063-d_{24}. The free mOX063-d_{24} contained a superhyperfine interaction with the amide nitrogen (a^N ∼ 220 mG) on the linker, depicted as a partially resolved triplet splitting of the ESR lineshape. This nitrogen hyperfine is consistent with the previously published trityls with ^{14}N-containing linkers.[79,90,91] After mOX063-d_{24} reacted with GB1, the superhyperfine nitrogen was broadened and unresolved due to the slower tumbling rate upon protein binding, as seen in Figure 3B.[79] However, the tumbling rate after protein binding is still rapid enough to resolve the satellite ^{13}C peaks in the CW ESR spectrum of GB1-bound mOX063-d_{24}, as seen in Figure 3A. This behavior has been described in a previous report of OX063-d_{24} spin label.[79] Spin counting of the mOX063-d_{24}-GB1 CW ESR spectrum yields a spin concentration of 203 μM. Given the protein concentration of 106 μM, these results indicate a labeling efficiency of 95%, which agrees with the UV−vis data.

More importantly, the mOX063-d_{24}-GB1 CW ESR spectrum can be fitted with a narrow single-component simulation without a broad component, commonly seen when using FT.[74,75,78,92] FT's broad component has been attributed to aggregated species of FT[76,77] and nonspecific binding in proteins[75,76,79,93] and membranes.[74] As a result, when using the simple spin-labeling workflow, FT had labeling efficiencies of 24−80% depending on the linker and protein.[67,78,79,92] On the other hand, mOX063-d_{24} is highly soluble and does not bind nonspecifically.[79] Therefore, the hydrophilicity of mOX063-d_{24}

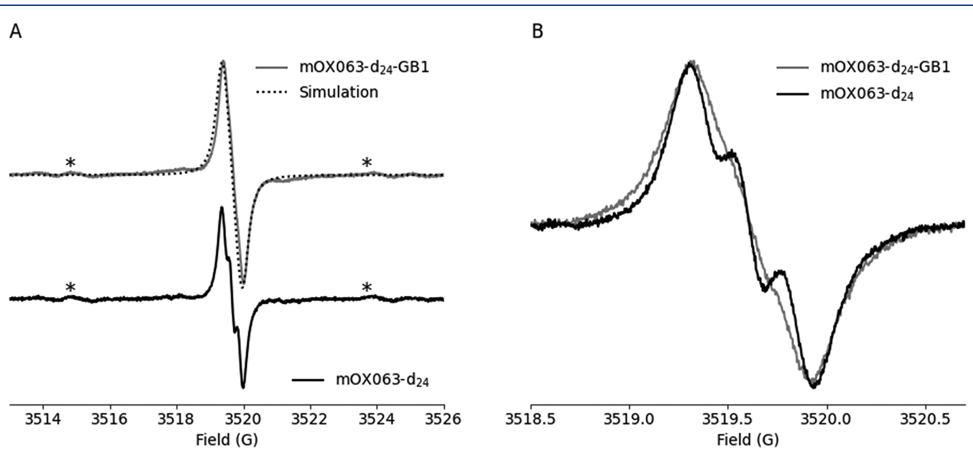

Figure 3. (A) CW−ESR spectra of mOX063-d_{24}-GB1 (top) and mOX063-d_{24} (bottom). The spectrum of mOX063-d_{24}-GB1 can be fitted with a narrow single-component simulation. The ^{13}C satellite peaks are marked with *. (B) CW−ESR spectra of mOX063-d_{24}-GB1 and mOX063-d_{24} with the observation window ∼2 G at the central lineshape. The nitrogen superhyperfine is partially resolved in the mOX063-d_{24} spectrum but not in the mOX063-d_{24}-GB1 spectrum.

https://doi.org/10.1021/acs.jpcb.1c02371
J. Phys. Chem. B XXXX, XXX, XXX−XXX

allows ~100% labeling efficiency using simple protein-labeling protocols. Additionally, the labeling efficiency of mOX063-d_{24} is slightly improved from the previously developed hydrophilic trityl spin label, Ox-SLIM, which is reported to have 85% labeling efficiency.[80] Such differences in labeling efficiency could be due to the difference in maleimide linker length between mOX063-d_{24} and Ox-SLIM and potentially to the differences in solvent accessibilities between the two sites in the two proteins.

Next, pulsed-ESR was used to measure the relaxation times of GB1-bound mOX063-d_{24} since these are critical parameters that dictate the efficacy of the label in pulsed dipolar spectroscopy. These data were acquired at a spin concentration of 5 μM and the sample was prepared in 20 mM PBS buffer at pH 7.4 and contained 20% glycerol. The phase-memory relaxation time (T_m) was measured by echo decay experiments. The measured values of T_m are listed in Table 1 and the data is shown in Figure S4A. The T_m of GB1-bound mOX063-d_{24} is 5.1, 4.3, or 3.6 μs at 80, 150, or 180 K, respectively. These relaxation measurements provided additional data points to the existing measurements from previous studies of OX063-based spin labels (cf. Table S1). For comparison, the T_m value of 5.1 μs for GB1-bound mOX063-d_{24} at 80 K is longer than the T_m value of 1.6 μs for protein-bound FT at 80 K.[78] The longest reported T_m of protein-bound FT is 2.9 μs at 50 K.[79] Increasing the T_m can both increase the echo intensity for distance measurements and increase the range of feasible temperature of the experiment.

Table 1. T_m and T_1 Measurements of mOX063-d_{24}-GB1 at 80, 150, and 180 K

temperature (K)	T_m (μs)	T_1 (ms)
80	5.1	1.98
150	4.3	0.175
180	3.6	0.112

At higher temperatures, mOX063-d_{24} also benefits from the shortening of T_1. GB1-bound mOX063-d_{24} has T_1 values of 1.98, 0.175, and 0.112 ms at 80, 150, and 180 K, respectively (Table 1 and Figure S4B,C). The mechanism for T_1 relaxation of trityl radicals as a function of temperature has been previously studied.[94] As T_1 gets shorter with increasing temperature, the amount of time required for GB1-bound mOX063-d_{24} to completely relax becomes shorter, leading to a faster rate of repeating the measurement. For comparison, the T_1 value of 1.98 ms for GB1-bound mOX063-d_{24} at 80 K listed in Table 1 is slightly longer than the T_1 value of 1.7 ms for protein-bound FT at 80 K.[78] However, distance measurements using FT are typically done at 50 K or lower, which has T_1 values of 6.3 ms or longer.[78] Therefore, distance measurement using mOX063-d_{24} at higher temperature leads to more scans per unit of time than the distance measurement using FT at the typical temperature of 50 K. Consequently, we expect that distance measurements using mOX063-d_{24} at higher temperatures benefit from a shorter T_1.

To showcase the sensitivity of mOX063-d_{24}, DQC experiments at 80 K or 150 K were performed on E15C/K28C GB1 doubly labeled by mOX063-d_{24}, as shown in Figure 4A. The method to measure SNR is described in the methods section. The DQC time trace achieved sufficiently high SNR at 150 K within approximately 1.5 h of runtime (SNR = 20 min$^{-1/2}$). On the other hand, at 80 K, even after 2 h of runtime, the

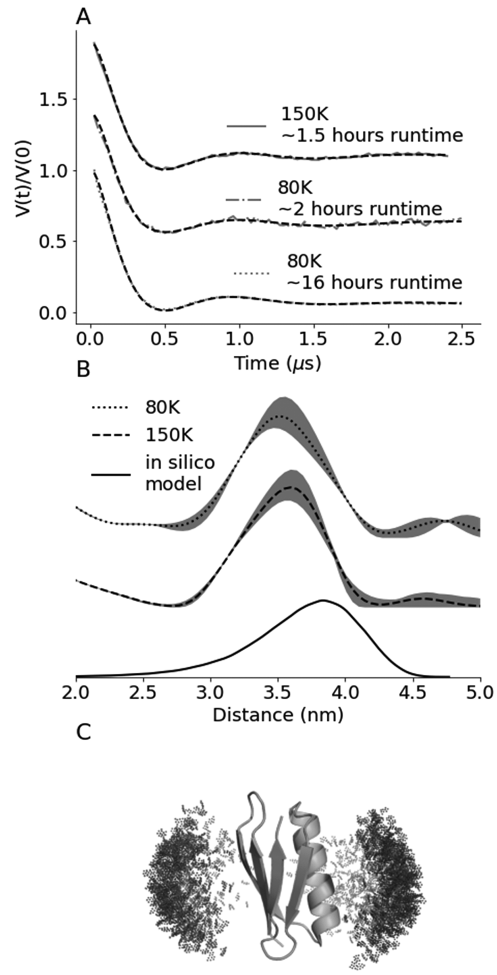

Figure 4. (A) DQC time traces of doubly labeled mOX063-d_{24}-GB1 at 150 K after 1.5 h of runtime and at 80 K after 2 and 16 h of runtime. (B) Distance distributions obtained from the 150 and 80 K DQC time traces using DeerAnalysis. The gray regions represent the error obtained from the validation function in DeerAnalysis. Additionally, a distance distribution was also obtained from *in silico* modeling using MTSSLWizard. (C) *In silico* model from MTSSLWizard using GB1 (PDB:2QMT) and mOX063-d_{24}. The two clusters represent the space occupied by the radical carbon.

DQC time trace (SNR = 7 min$^{-1/2}$) is noisier than the 150 K DQC time trace. The higher SNR of 150 K DQC than the SNR of 80 K DQC can be rationalized by the following analysis of SNR for pulsed-ESR experiments[95]

$$\mathrm{SNR}(T) \propto \frac{1}{T}\exp[-t_{\mathrm{tot}}/T_m(T)]\sqrt{\frac{1}{T_1(T)}} \quad (1)$$

where T is the temperature and t_{tot} is the amount of time the electron coherence evolves until the detection of the echo signal. The $1/T$ term in eq 1 is due to the Boltzmann factor.[96] Based on eq 1, the shorter T_1 = 0.175 ms at 150 K than the T_1 = 1.98 ms at 80 K (Table 1, Figures S4B, and S5C) contributes to 3.36 times improvement in SNR. On the other hand, the increase in temperature from 80 to 150 K only led to a slight reduction of T_m from 5.1 to 4.3 μs. Furthermore, the increase in temperature causes a loss in echo intensity due to the reduction in spin polarization. Based on eq 1, the decrease in T_m and spin polarization reduces the SNR by 0.43 times. As a result, the final SNR at 150 K is 3.36 × 0.43 = 1.44 times

https://doi.org/10.1021/acs.jpcb.1c02371
J. Phys. Chem. B XXXX, XXX, XXX−XXX

higher than the SNR at 80 K. We can see the SNR improvement from the DQC echo comparison between 80 and 150 K, as shown in Figure S5. Overall, the gain in sensitivity due to T_1 was able to overcompensate the loss of echo intensity from the shortening of T_m and the reduction of spin polarization. However, increasing the temperature further to 180 K causes the reduction in sensitivity due to reduced spin polarization and T_m. For example, the sensitivity at 180 K is ~79% of the sensitivity at 150 K based on eq 1. These comparisons signify the importance of experimentally evaluating the relaxation times at various temperatures, since the values can be different for different systems. While 80 K is not the most optimal temperature for mOX063-d_{24} DQC, its SNR = 7 $min^{-1/2}$ is comparable to the reported FT's SNR[78] ranging from 7 to 8.9 $min^{-1/2}$ at 50 K. These comparisons of SNR exemplify the sensitivity gained from performing mOX063-d_{24} DQC experiments at the optimal temperature.

We analyzed the time traces using the DeerAnalysis 2018[87] package and the Tikhonov regularization method to extract the distance distributions shown in Figure 4B. Expectedly, at both temperatures, the distance distributions were close to identical, with the most probable distance of 3.6 nm. To predict the distance distribution, we built an *in silico* model using MTSSLWizard.[97] Since the mOX063-d_{24} spin label does not exist in the MTSSLWizard package, we first implemented the mOX063-d_{24} model into the MTSSLWizard software. Details are provided in Figure S6. The model predicted that the most probable distance is 3.8 nm, as shown in Figure 4B, which is in reasonable agreement with the DQC results. Furthermore, the experimental results have a standard deviation of ~0.6 nm, which is on par with the standard deviation of ~0.8 nm obtained using nitroxide on the same GB1 mutant.[85]

After the *in vitro* experiments, the viability of mOX063-d_{24} for *in-cell* experiments was explored. Specifically, the mOX063-d_{24}-GB1 (200 μM of spins) was subjected to either 10 times excess of ascorbic acid or the cytosol extract of *X. laevis* (African Bullfrog) oocytes. The cytosol was extracted from oocytes using the previously published protocol.[85] The signal intensity of mOX063-d_{24} was monitored over time using CW−ESR, and the maximum intensity of each spectrum was plotted against time in Figure 5A. The signal intensity decays to about 97 and 95% of its original intensity in ascorbate and the cytosol after 5 h, respectively. The stability of mOX063-d_{24} is on par with the stability of other trityls.[73,80] The signal persistence of mOX063-d_{24} showcases the reduction resistance of mOX063-d_{24} against the cytosolic antioxidants that play a role in reducing radicals *in-cell*.[98]

After measuring the mOX063-d_{24} stability, mOX063-d_{24}-GB1 was injected into oocytes and incubated for 30 min after injection before flash-freezing the sample. The 30 min incubation allows for mOX063-d_{24}-GB1 to completely diffuse in oocytes.[48] The echo decay experiment measured the T_m of mOX063-d_{24} at 80 K in oocytes to be 4.3 μs, as shown in Figure S7, which is shorter than the T_m of mOX063-d_{24} *in vitro*, as shown in Table 1 and Figure S4A. The lower GB1-bound mOX063-d_{24} T_m *in-cell* compared to *in vitro* was expected because of the crowded environment *in-cell*. The crowded environment can lead to an increase in the local concentration of protons near the radical, which enhances the contribution of electron−nuclei interactions to relaxation. In addition, the presence of paramagnetic metal ions, primarily Mn(II),[99] in the cell can enhance relaxation. However, the T_m of mOX063-d_{24} in oocytes is surprising since previous reports

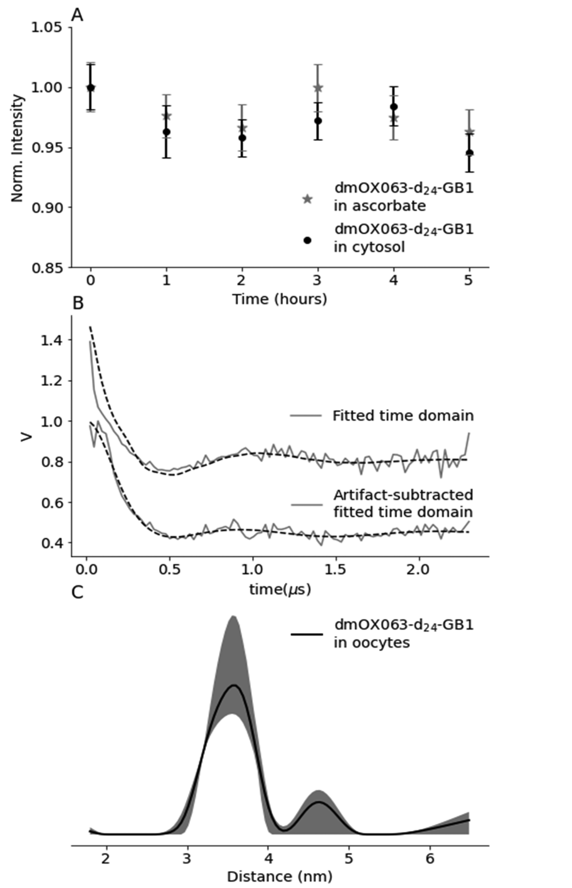

Figure 5. (A) Plot of the maximum intensity of the CW-ESR spectrum of doubly labeled mOX063-d_{24}-GB1 vs time in 10 times excess of ascorbate or the cytosol extracted from *X. laevis* oocytes. The height of the vertical bars represents the RMSD in the CW ESR spectrum. (B) DQC time trace of mOX063-d_{24}-GB1 at the 80 K Q-band before and after artifact subtraction. (C) Distance distribution (most probable distance of 3.6 nm) extracted from the artifact-subtracted time-domain signal using DeerAnalysis. The gray region represents the error obtained from the validation function.

of other organic spin labels used *in-cell* (nitroxides[50,57,100] and FT[67,72,73]) have T_m values in the range of 0.6−2 μs. Therefore, mOX063-d_{24} also improves the sensitivity of distance measurements *in-cell* due to the T_m that is at least 2 times longer than previously published T_m of nitroxide or FT *in-cell*.

Distance measurements of mOX063-d_{24}-GB1 in oocytes were done using DQC at 80 K, as shown in Figure 5B. We observed an artifact that overlaps the desired DQC signal at zero time. Such an artifact has been seen previously and attributed to trityl dimers and to partial labeling of noncysteine residues such as lysine.[101] We repeated the labeling procedure on WT GB1 that has no cysteine residues. After concentrating the sample, UV−vis measurement indicates no presence of mOX063-d_{24}, as shown in Figure S8. We expected this result since our previous work using GB1 and maleimide-linked nitroxide (5-MSL) did not show overlabeling of the protein.[85] In addition, we did not see an ESR signal from the WT GB1 sample, as shown in Figure S9, which also excludes the presence of dimers.

We attribute this artifact to the formation of a small echo generated by the first and the fourth pulses in the DQC 6-pulse sequence. This interference can be readily seen in the two-dimensional (2D) contour plot of the DQC signal, as shown in

https://doi.org/10.1021/acs.jpcb.1c02371
J. Phys. Chem. B XXXX, XXX, XXX−XXX

Figure S9A. As a result, the DQC time trace contained an artifact shown as a sharp feature at the $t = 0$, as shown in Figure S10B, which led to improper fitting of the time trace. Additionally, the artifact contributed to a short distance around 2 nm, as shown in Figure S11A. The artifact seemed to be a result of inefficient phase cycling in our DQC experiment and is evident in the in-cell data due to the lower SNR.

To support this hypothesis, we performed the DQC experiment using the same parameters on 300 μM TEMPOL, as shown in Figure S12. The same artifact was seen crossing the desired DQC echo at a slanted angle shown in the 2D contour plot in Figure S12A. As a result, a sharp feature at $t = 0$ manifested, as shown in Figure S12B. This artifact has not been seen in previous works. The artifact was more prominent in the *in-cell* experiment than in the *in vitro* experiment for two reasons. First, the measured echo in the *in-cell* DQC was half as intense as the measured echo in the *in vitro* DQC. The lower *in-cell* echo intensity is due to the shorter T_m *in-cell* than the T_m *in vitro*. Additionally, reduction of mOX063-d_{24} can still occur due to the contribution of membrane-associated proteins[85] such as thioredoxin[102] and glutathione reductase,[103] which are not accounted for in our cytosol stability measurement. These two contributions led to a less intense measured echo, causing the artifact to be prominent in the *in-cell* DQC.

To remove the artifact in the DQC time trace in oocytes, DQC was performed on a sample of free mOX063-d_{24}, which contained only the artifact shown in Figure S10B. The free mOX063-d_{24} DQC time trace was used to subtract the artifact from the time trace of mOX063-d_{24}-GB1 in oocytes, as shown in Figure 5B. The artifact-subtracted time trace was used to extract the distance distribution shown in Figure 5C, which agrees quite well with the *in vitro* distance measurements in Figure 4B. Furthermore, we were able to repeat the *in-cell* DQC experiment at 150 K, as shown in Figure S13, and obtain a similar distribution as the 80 K *in-cell* distribution. Additionally, we repeated our *in-cell* experiments at 80 K using a different batch of oocytes and newly overexpressed and labeled GB1 to ensure that the *in-cell* results are reproducible. This data is shown in Figure S14. Overall, we obtained a highly sensitive distance measurement in oocytes using mOX063-d_{24}.

CONCLUSIONS

In conclusion, this work showed that mOX063-d_{24} has a high protein-labeling efficiency of ~97%. Furthermore, we showed that *in vitro* distance measurements of mOX063-d_{24} are more sensitive at higher temperatures. Finally, we obtained distance measurements using mOX063-d_{24} *in-cell*, which agree with *in silico* modeling. This work adds to the library of spin labels that can be used for *in-cell* work. In particular, mOX063-d_{24} is similar to Ox-SLIM[80] since both are hydrophilic spin labels with a maleimide linker, as shown in Figure 1A. However, these two spin labels differ in their trityl cores and linker lengths. These differences provide variation in the labeling efficiency, T_m, and breadth of distance distribution. In one case, Ox-SLIM's short linker length can provide narrow distance distributions that can readily resolve different protein conformations.[73,80] On the other hand, mOX063-d_{24} provides longer T_m and higher labeling efficiency leading to the sensitivity improvement in the distance measurements. Overall, Ox-SLIM and mOX063-d_{24} are complementary to each other due to their differences.

ASSOCIATED CONTENT

Supporting Information

The Supporting Information is available free of charge at https://pubs.acs.org/doi/10.1021/acs.jpcb.1c02371.

HRMS-ESI data of mOX063-d_{24} and mOX063-d_{24}-GB1, UV–vis spectra of mOX063-d_{24} + WT GB1, pulsed-ESR relaxation measurements, details of MtsslWizard modeling, comparison of *in vitro* DQC echo of mOX063-d_{24}-GB1 at 80 and 150 K, raw one-dimensional (1D) and 2D DQC time domains, *in-cell* DQC data at 150 and 80 K (second trial) (PDF)

AUTHOR INFORMATION

Corresponding Authors

Benoit Driesschaert – *Department of Pharmaceutical Sciences, School of Pharmacy & In Vivo Multifunctional Magnetic Resonance (IMMR) Center, Health Sciences Center, West Virginia University, Morgantown, West Virginia 26506, United States;* orcid.org/0000-0002-1402-413X; Email: benoit.driesschaert@hsc.wvu.edu

Sunil Saxena – *Department of Chemistry, University of Pittsburgh, Pittsburgh, Pennsylvania 15260, United States;* orcid.org/0000-0001-9098-6114; Email: sksaxena@pitt.edu

Authors

Zikri Hasanbasri – *Department of Chemistry, University of Pittsburgh, Pittsburgh, Pennsylvania 15260, United States*

Kevin Singewald – *Department of Chemistry, University of Pittsburgh, Pittsburgh, Pennsylvania 15260, United States*

Teresa D. Gluth – *Department of Pharmaceutical Sciences, School of Pharmacy & In Vivo Multifunctional Magnetic Resonance (IMMR) Center, Health Sciences Center, West Virginia University, Morgantown, West Virginia 26506, United States*

Complete contact information is available at: https://pubs.acs.org/10.1021/acs.jpcb.1c02371

Notes

The authors declare no competing financial interest.

ACKNOWLEDGMENTS

This work was partially supported by the NIH grants (USA) R00EB023990, R21EB028553-01A1, and NSF-BSF MCB 2001654. Z.H. acknowledges fellowship support from NIH T32 GM 88119-9. The content is solely the responsibility of the authors and does not necessarily represent the official views of the NIH. We acknowledge the use of the WVU Shared Research Facilities. The authors would like to acknowledge Stephen E. White, who gathered and analyzed the ESI-MS data for mOX063-d_{24}-GB1.

REFERENCES

(1) Dhar, A.; Girdhar, K.; Singh, D.; Gelman, H.; Ebbinghaus, S.; Gruebele, M. Protein stability and folding kinetics in the nucleus and endoplasmic reticulum of eucaryotic cells. *Biophys. J.* **2011**, *101*, 421–430.

(2) Ignatova, Z.; Krishnan, B.; Bombardier, J. P.; Marcelino, A. M. C.; Hong, J.; Gierasch, L. M. From the test tube to the cell: exploring the folding and aggregation of a beta-clam protein. *Biopolymers* **2007**, *88*, 157–163.

(3) Cheung, M. S.; Gasic, A. G. Towards developing principles of protein folding and dynamics in the cell. *Phys. Biol.* **2018**, *15*, No. 063001.
(4) Timr, S.; Madern, D.; Sterpone, F. Protein thermal stability. *Prog. Mol. Biol. Transl. Sci.* **2020**, *170*, 239−272.
(5) Sukenik, S.; Salam, M.; Wang, Y.; Gruebele, M. In-Cell Titration of Small Solutes Controls Protein Stability and Aggregation. *J. Am. Chem. Soc.* **2018**, *140*, 10497−10503.
(6) Silverstein, T. P.; Slade, K. Effects of macromolecular crowding on biochemical systems. *J. Chem. Educ.* **2019**, *96*, 2476−2487.
(7) Gao, M.; Held, C.; Patra, S.; Arns, L.; Sadowski, G.; Winter, R. Crowders and Cosolvents-Major Contributors to the Cellular Milieu and Efficient Means to Counteract Environmental Stresses. *ChemPhysChem* **2017**, *18*, 2951−2972.
(8) Feng, R.; Gruebele, M.; Davis, C. M. Quantifying protein dynamics and stability in a living organism. *Nat. Commun.* **2019**, *10*, No. 1179.
(9) König, I.; Zarrine-Afsar, A.; Aznauryan, M.; Soranno, A.; Wunderlich, B.; Dingfelder, F.; Stüber, J. C.; Plückthun, A.; Nettels, D.; Schuler, B. Single-molecule spectroscopy of protein conformational dynamics in live eukaryotic cells. *Nat. Methods* **2015**, *12*, 773−779.
(10) Senske, M.; Törk, L.; Born, B.; Havenith, M.; Herrmann, C.; Ebbinghaus, S. Protein stabilization by macromolecular crowding through enthalpy rather than entropy. *J. Am. Chem. Soc.* **2014**, *136*, 9036−9041.
(11) Shahid, S.; Ahmad, F.; Hassan, M. I.; Islam, A. Relationship between protein stability and functional activity in the presence of macromolecular crowding agents alone and in mixture: An insight into stability-activity trade-off. *Arch. Biochem. Biophys.* **2015**, *584*, 42−50.
(12) Cook, E. C.; Creamer, T. P. Calcineurin in a crowded world. *Biochemistry* **2016**, *55*, 3092−3101.
(13) Yang, Y.; Chen, S.-N.; Yang, F.; Li, X.-Y.; Feintuch, A.; Su, X.-C.; Goldfarb, D. In-cell destabilization of a homodimeric protein complex detected by DEER spectroscopy. *Proc. Natl. Acad. Sci. U.S.A.* **2020**, *117*, 20566−20575.
(14) Guseman, A. J.; Perez Goncalves, G. M.; Speer, S. L.; Young, G. B.; Pielak, G. J. Protein shape modulates crowding effects. *Proc. Natl. Acad. Sci. U.S.A.* **2018**, *115*, 10965−10970.
(15) Berg, O. G. The influence of macromolecular crowding on thermodynamic activity: solubility and dimerization constants for spherical and dumbbell-shaped molecules in a hard-sphere mixture. *Biopolymers* **1990**, *30*, 1027−1037.
(16) Goldfarb, D. Gd3+ spin labeling for distance measurements by pulse EPR spectroscopy. *Phys. Chem. Chem. Phys.* **2014**, *16*, 9685−9699.
(17) Hubbell, W. L.; López, C. J.; Altenbach, C.; Yang, Z. Technological advances in site-directed spin labeling of proteins. *Curr. Opin. Struct. Biol.* **2013**, *23*, 725−733.
(18) Roser, P.; Schmidt, M. J.; Drescher, M.; Summerer, D. Site-directed spin labeling of proteins for distance measurements in vitro and in cells. *Org. Biomol. Chem.* **2016**, *14*, 5468−5476.
(19) Gamble Jarvi, A.; Bogetti, X.; Singewald, K.; Ghosh, S.; Saxena, S. Going the dHis-tance: Site-Directed Cu2+ Labeling of Proteins and Nucleic Acids. *Acc. Chem. Res.* **2021**, *54*, 1481−1491.
(20) Singewald, K.; Bogetti, X.; Sinha, K.; Rule, G. S.; Saxena, S. Double Histidine Based EPR Measurements at Physiological Temperatures Permit Site-Specific Elucidation of Hidden Dynamics in Enzymes. *Angew. Chem., Int. Ed.* **2020**, *59*, 23040−23044.
(21) Altenbach, C.; López, C. J.; Hideg, K.; Hubbell, W. L. Exploring Structure, Dynamics, and Topology of Nitroxide Spin-Labeled Proteins Using Continuous-Wave Electron Paramagnetic Resonance Spectroscopy. *Methods Enzymol.* **2015**, *564*, 59−100.
(22) Saxena, S.; Freed, J. H. Theory of double quantum two-dimensional electron spin resonance with application to distance measurements. *J. Chem. Phys.* **1997**, *107*, 1317−1340.
(23) Borbat, P. P.; Freed, J. H. Multiple-quantum ESR and distance measurements. *Chem. Phys. Lett.* **1999**, *313*, 145−154.
(24) Milov, A. D.; Maryasov, A. G.; Tsvetkov, Y. D. Pulsed electron double resonance (PELDOR) and its applications in free-radicals research. *Appl. Magn. Reson.* **1998**, *15*, 107−143.
(25) Pannier, M.; Veit, S.; Godt, A.; Jeschke, G.; Spiess, H. W. Dead-time free measurement of dipole-dipole interactions between electron spins. *J. Magn. Reson.* **2000**, *142*, 331−340.
(26) Jeschke, G.; Pannier, M.; Godt, A.; Spiess, H. W. Dipolar spectroscopy and spin alignment in electron paramagnetic resonance. *Chem. Phys. Lett.* **2000**, *331*, 243−252.
(27) Kulik, L. V.; Dzuba, S. A.; Grigoryev, I. A.; Tsvetkov, Y. D. Electron dipole−dipole interaction in ESEEM of nitroxide biradicals. *Chem. Phys. Lett.* **2001**, *343*, 315−324.
(28) Milikisyants, S.; Scarpelli, F.; Finiguerra, M. G.; Ubbink, M.; Huber, M. A pulsed EPR method to determine distances between paramagnetic centers with strong spectral anisotropy and radicals: the dead-time free RIDME sequence. *J. Magn. Reson.* **2009**, *201*, 48−56.
(29) Assafa, T. E.; Anders, K.; Linne, U.; Essen, L.-O.; Bordignon, E. Light-Driven Domain Mechanics of a Minimal Phytochrome Photosensory Module Studied by EPR. *Structure* **2018**, *26*, 1534−1545.e4.
(30) Liu, Z.; Casey, T. M.; Blackburn, M. E.; Huang, X.; Pham, L.; de Vera, I. M. S.; Carter, J. D.; Kear-Scott, J. L.; Veloro, A. M.; Galiano, L.; et al. Pulsed EPR characterization of HIV-1 protease conformational sampling and inhibitor-induced population shifts. *Phys. Chem. Chem. Phys.* **2016**, *18*, 5819−5831.
(31) Grytz, C. M.; Marko, A.; Cekan, P.; Sigurdsson, S. T.; Prisner, T. F. Flexibility and conformation of the cocaine aptamer studied by PELDOR. *Phys. Chem. Chem. Phys.* **2016**, *18*, 2993−3002.
(32) Hänelt, I.; Wunnicke, D.; Bordignon, E.; Steinhoff, H.-J.; Slotboom, D. J. Conformational heterogeneity of the aspartate transporter Glt(Ph). *Nat. Struct. Mol. Biol.* **2013**, *20*, 210−214.
(33) Dalmas, O.; Sompornpisut, P.; Bezanilla, F.; Perozo, E. Molecular mechanism of Mg2+-dependent gating in CorA. *Nat. Commun.* **2014**, *5*, No. 3590.
(34) Verhalen, B.; Dastvan, R.; Thangapandian, S.; Peskova, Y.; Koteiche, H. A.; Nakamoto, R. K.; Tajkhorshid, E.; Mchaourab, H. S. Energy transduction and alternating access of the mammalian ABC transporter P-glycoprotein. *Nature* **2017**, *543*, 738−741.
(35) Dawidowski, D.; Cafiso, D. S. Munc18-1 and the Syntaxin-1 N Terminus Regulate Open-Closed States in a t-SNARE Complex. *Structure* **2016**, *24*, 392−400.
(36) Sameach, H.; Ghosh, S.; Gevorkyan-Airapetov, L.; Saxena, S.; Ruthstein, S. EPR spectroscopy detects various active state conformations of the transcriptional regulator cuer. *Angew. Chem., Int. Ed.* **2019**, *58*, 3053−3056.
(37) Stone, K.; Townsend, J.; Sarver, J.; Sapienza, P.; Saxena, S.; Jen-Jacobson, L. Electron Spin Resonance Shows Common Structural Features for Different Classes of Eco RI-DNA Complexes. *Angew. Chem., Int. Ed.* **2008**, *120*, 10346−10348.
(38) Milikisiyants, S.; Wang, S.; Munro, R. A.; Donohue, M.; Ward, M. E.; Bolton, D.; Brown, L. S.; Smirnova, T. I.; Ladizhansky, V.; Smirnov, A. I. Oligomeric Structure of Anabaena Sensory Rhodopsin in a Lipid Bilayer Environment by Combining Solid-State NMR and Long-range DEER Constraints. *J. Mol. Biol.* **2017**, *429*, 1903−1920.
(39) Park, S.-Y.; Borbat, P. P.; Gonzalez-Bonet, G.; Bhatnagar, J.; Pollard, A. M.; Freed, J. H.; Bilwes, A. M.; Crane, B. R. Reconstruction of the chemotaxis receptor-kinase assembly. *Nat. Struct. Mol. Biol.* **2006**, *13*, 400−407.
(40) Valera, S.; Ackermann, K.; Pliotas, C.; Huang, H.; Naismith, J. H.; Bode, B. E. Accurate extraction of nanometer distances in multimers by pulse EPR. *Chem. - Eur. J* **2016**, *22*, 4700−4703.
(41) DeBerg, H. A.; Bankston, J. R.; Rosenbaum, J. C.; Brzovic, P. S.; Zagotta, W. N.; Stoll, S. Structural mechanism for the regulation of HCN ion channels by the accessory protein TRIP8b. *Structure* **2015**, *23*, 734−744.
(42) Upadhyay, A. K.; Borbat, P. P.; Wang, J.; Freed, J. H.; Edmondson, D. E. Determination of the oligomeric states of human and rat monoamine oxidases in the outer mitochondrial membrane and octyl beta-D-glucopyranoside micelles using pulsed dipolar

electron spin resonance spectroscopy. *Biochemistry* **2008**, *47*, 1554−1566.
(43) Yin, D. M.; Hannam, J. S.; Schmitz, A.; Schiemann, O.; Hagelueken, G.; Famulok, M. Studying the Conformation of a Receptor Tyrosine Kinase in Solution by Inhibitor-Based Spin Labeling. *Angew. Chem., Int. Ed.* **2017**, *56*, 8417−8421.
(44) Gamble Jarvi, A.; Cunningham, T. F.; Saxena, S. Efficient localization of a native metal ion within a protein by Cu2+-based EPR distance measurements. *Phys. Chem. Chem. Phys.* **2019**, *21*, 10238−10243.
(45) Abdullin, D.; Florin, N.; Hagelueken, G.; Schiemann, O. EPR-based approach for the localization of paramagnetic metal ions in biomolecules. *Angew. Chem., Int. Ed.* **2015**, *54*, 1827−1831.
(46) Ketter, S.; Gopinath, A.; Rogozhnikova, O.; Trukhin, D.; Tormyshev, V. M.; Bagryanskaya, E. G.; Joseph, B. In Situ Labeling and Distance Measurements of Membrane Proteins in *E. coli* Using Finland and OX063 Trityl Labels. *Chem. - Eur. J* **2021**, *27*, 2299−2304.
(47) Igarashi, R.; Sakai, T.; Hara, H.; Tenno, T.; Tanaka, T.; Tochio, H.; Shirakawa, M. Distance determination in proteins inside *Xenopus laevis* oocytes by double electron-electron resonance experiments. *J. Am. Chem. Soc.* **2010**, *132*, 8228−8229.
(48) Lawless, M. J.; Shimshi, A.; Cunningham, T. F.; Kinde, M. N.; Tang, P.; Saxena, S. Analysis of Nitroxide-Based Distance Measurements in Cell Extracts and in Cells by Pulsed ESR Spectroscopy. *ChemPhysChem* **2017**, *18*, 1653−1660.
(49) Wojciechowski, F.; Groß, A.; Holder, I. T.; Knörr, L.; Drescher, M.; Hartig, J. S. Pulsed EPR spectroscopy distance measurements of DNA internally labelled with Gd(3+)-DOTA. *Chem. Commun.* **2015**, *51*, 13850−13853.
(50) Krstić, I.; Hänsel, R.; Romainczyk, O.; Engels, J. W.; Dötsch, V.; Prisner, T. F. Long-range distance measurements on nucleic acids in cells by pulsed EPR spectroscopy. *Angew. Chem., Int. Ed.* **2011**, *50*, 5070−5074.
(51) Azarkh, M.; Okle, O.; Eyring, P.; Dietrich, D. R.; Drescher, M. Evaluation of spin labels for in-cell EPR by analysis of nitroxide reduction in cell extract of *Xenopus laevis* oocytes. *J. Magn. Reson.* **2011**, *212*, 450−454.
(52) Schmidt, M. J.; Fedoseev, A.; Bücker, D.; Borbas, J.; Peter, C.; Drescher, M.; Summerer, D. EPR Distance Measurements in Native Proteins with Genetically Encoded Spin Labels. *ACS Chem. Biol.* **2015**, *10*, 2764−2771.
(53) Fleissner, M. R.; Brustad, E. M.; Kálai, T.; Altenbach, C.; Cascio, D.; Peters, F. B.; Hideg, K.; Peuker, S.; Schultz, P. G.; Hubbell, W. L. Site-directed spin labeling of a genetically encoded unnatural amino acid. *Proc. Natl. Acad. Sci. U.S.A.* **2009**, *106*, 21637−21642.
(54) Mascali, F. C.; Ching, H. Y. V.; Rasia, R. M.; Un, S.; Tabares, L. C. Using Genetically Encodable Self-Assembling Gd(III) Spin Labels To Make In-Cell Nanometric Distance Measurements. *Angew. Chem., Int. Ed.* **2016**, *55*, 11041−11043.
(55) Kucher, S.; Korneev, S.; Tyagi, S.; Apfelbaum, R.; Grohmann, D.; Lemke, E. A.; Klare, J. P.; Steinhoff, H.-J.; Klose, D. Orthogonal spin labeling using click chemistry for in vitro and in vivo applications. *J. Magn. Reson.* **2017**, *275*, 38−45.
(56) Kugele, A.; Silkenath, B.; Langer, J.; Wittmann, V.; Drescher, M. Protein Spin Labeling with a Photocaged Nitroxide Using Diels-Alder Chemistry. *ChemBioChem* **2019**, *20*, 2479−2484.
(57) Karthikeyan, G.; Bonucci, A.; Casano, G.; Gerbaud, G.; Abel, S.; Thomé, V.; Kodjabachian, L.; Magalon, A.; Guigliarelli, B.; Belle, V.; et al. A Bioresistant Nitroxide Spin Label for In-Cell EPR Spectroscopy: In Vitro and In Oocytes Protein Structural Dynamics Studies. *Angew. Chem., Int. Ed.* **2018**, *57*, 1366−1370.
(58) Paletta, J. T.; Pink, M.; Foley, B.; Rajca, S.; Rajca, A. Synthesis and reduction kinetics of sterically shielded pyrrolidine nitroxides. *Org. Lett.* **2012**, *14*, 5322−5325.
(59) Qi, M.; Gross, A.; Jeschke, G.; Godt, A.; Drescher, M. Gd(III)-PyMTA label is suitable for in-cell EPR. *J. Am. Chem. Soc.* **2014**, *136*, 15366−15378.
(60) Martorana, A.; Bellapadrona, G.; Feintuch, A.; Di Gregorio, E.; Aime, S.; Goldfarb, D. Probing protein conformation in cells by EPR distance measurements using Gd3+ spin labeling. *J. Am. Chem. Soc.* **2014**, *136*, 13458−13465.
(61) Thonon, D.; Jacques, V.; Desreux, J. F. Relaxivity properties and conjugation with albumin and thiolated particles. *Contrast Media Mol. Imaging* **2007**, *2*, 24−34. A gadolinium triacetic monoamide DOTA derivative with a methanethiosulfonate anchor group.
(62) Shevelev, G. Y.; Krumkacheva, O. A.; Lomzov, A. A.; Kuzhelev, A. A.; Trukhin, D. V.; Rogozhnikova, O. Y.; Tormyshev, V. M.; Pyshnyi, D. V.; Fedin, M. V.; Bagryanskaya, E. G. Triarylmethyl labels: toward improving the accuracy of EPR nanoscale distance measurements in dnas. *J. Phys. Chem. B* **2015**, *119*, 13641−13648.
(63) Yang, Z.; Liu, Y.; Borbat, P.; Zweier, J. L.; Freed, J. H.; Hubbell, W. L. Pulsed ESR dipolar spectroscopy for distance measurements in immobilized spin labeled proteins in liquid solution. *J. Am. Chem. Soc.* **2012**, *134*, 9950−9952.
(64) Reginsson, G. W.; Kunjir, N. C.; Sigurdsson, S. T.; Schiemann, O. Trityl radicals: spin labels for nanometer-distance measurements. *Chem. - Eur. J* **2012**, *18*, 13580−13584.
(65) Dhimitruka, I.; Bobko, A. A.; Eubank, T. D.; Komarov, D. A.; Khramtsov, V. V. Phosphonated trityl probes for concurrent in vivo tissue oxygen and pH monitoring using electron paramagnetic resonance-based techniques. *J. Am. Chem. Soc.* **2013**, *135*, 5904−5910.
(66) Liu, W.; Nie, J.; Tan, X.; Liu, H.; Yu, N.; Han, G.; Zhu, Y.; Villamena, F. A.; Song, Y.; Zweier, J. L.; et al. Synthesis and characterization of pegylated trityl radicals: effect of pegylation on physicochemical properties. *J. Org. Chem.* **2017**, *82*, 588−596.
(67) Jassoy, J. J.; Berndhäuser, A.; Duthie, F.; Kühn, S. P.; Hagelueken, G.; Schiemann, O. Versatile Trityl Spin Labels for Nanometer Distance Measurements on Biomolecules In Vitro and within Cells. *Angew. Chem., Int. Ed.* **2017**, *56*, 177−181.
(68) Owenius, R.; Eaton, G. R.; Eaton, S. S. Frequency (250 MHz to 9.2 GHz) and viscosity dependence of electron spin relaxation of triarylmethyl radicals at room temperature. *J. Magn. Reson.* **2005**, *172*, 168−175.
(69) Khramtsov, V. V.; Bobko, A. A.; Tseytlin, M.; Driesschaert, B. Exchange phenomena in the electron paramagnetic resonance spectra of the nitroxyl and trityl radicals: multifunctional spectroscopy and imaging of local chemical microenvironment. *Anal. Chem.* **2017**, *89*, 4758−4771.
(70) Yang, Z.; Bridges, M. D.; López, C. J.; Rogozhnikova, O. Y.; Trukhin, D. V.; Brooks, E. K.; Tormyshev, V.; Halpern, H. J.; Hubbell, W. L. A triarylmethyl spin label for long-range distance measurement at physiological temperatures using T1 relaxation enhancement. *J. Magn. Reson.* **2016**, *269*, 50−54.
(71) Kuzhelev, A. A.; Krumkacheva, O. A.; Shevelev, G. Y.; Yulikov, M.; Fedin, M. V.; Bagryanskaya, E. G. Room-temperature distance measurements using RIDME and the orthogonal spin labels trityl/nitroxide. *Phys. Chem. Chem. Phys.* **2018**, *20*, 10224−10230.
(72) Yang, Y.; Pan, B.-B.; Tan, X.; Yang, F.; Liu, Y.; Su, X.-C.; Goldfarb, D. In-Cell Trityl-Trityl Distance Measurements on Proteins. *J. Phys. Chem. Lett.* **2020**, *11*, 1141−1147.
(73) Fleck, N.; Heubach, C. A.; Hett, T.; Haege, F. R.; Bawol, P. P.; Baltruschat, H.; Schiemann, O. SLIM: A Short-Linked, Highly Redox-Stable Trityl Label for High-Sensitivity In-Cell EPR Distance Measurements. *Angew. Chem., Int. Ed.* **2020**, *59*, 9767−9772.
(74) Joseph, B.; Tormyshev, V. M.; Rogozhnikova, O. Y.; Akhmetzyanov, D.; Bagryanskaya, E. G.; Prisner, T. F. Selective High-Resolution Detection of Membrane Protein-Ligand Interaction in Native Membranes Using Trityl-Nitroxide PELDOR. *Angew. Chem., Int. Ed.* **2016**, *55*, 11538−11542.
(75) Song, Y.; Liu, Y.; Liu, W.; Villamena, F. A.; Zweier, J. L. Characterization of the Binding of the Finland Trityl Radical with Bovine Serum Albumin. *RSC Adv.* **2014**, *4*, 47649−47656.
(76) Dhimitruka, I.; Velayutham, M.; Bobko, A. A.; Khramtsov, V. V.; Villamena, F. A.; Hadad, C. M.; Zweier, J. L. Large-scale synthesis of a persistent trityl radical for use in biomedical EPR applications and imaging. *Bioorg. Med. Chem. Lett.* **2007**, *17*, 6801−6805.

(77) Marin-Montesinos, I.; Paniagua, J. C.; Peman, A.; Vilaseca, M.; Luis, F.; Van Doorslaer, S.; Pons, M. Paramagnetic spherical nanoparticles by the self-assembly of persistent trityl radicals. *Phys. Chem. Chem. Phys.* **2016**, *18*, 3151−3158.

(78) Jassoy, J. J.; Heubach, C. A.; Hett, T.; Bernhard, F.; Haege, F. R.; Hagelueken, G.; Schiemann, O. Site Selective and Efficient Spin Labeling of Proteins with a Maleimide-Functionalized Trityl Radical for Pulsed Dipolar EPR Spectroscopy. *Molecules* **2019**, *24*, No. 2735.

(79) Tormyshev, V. M.; Chubarov, A. S.; Krumkacheva, O. A.; Trukhin, D. V.; Rogozhnikova, O. Y.; Spitsyna, A. S.; Kuzhelev, A. A.; Koval, V. V.; Fedin, M. V.; Godovikova, T. S.; et al. Methanethiosulfonate Derivative of OX063 Trityl: A Promising and Efficient Reagent for Side-Directed Spin Labeling of Proteins. *Chem. - Eur. J* **2020**, *26*, 2705−2712.

(80) Fleck, N.; Heubach, C.; Hett, T.; Spicher, S.; Grimme, S.; Schiemann, O. Ox-SLIM: Synthesis of and Site-Specific Labelling with a Highly Hydrophilic Trityl Spin Label. *Chem. - Eur. J* **2021**, *27*, 5292−5297.

(81) Girvin, M. E.; Fillingame, R. H. Determination of local protein structure by spin label difference 2D NMR: the region neighboring Asp61 of subunit c of the F1F0 ATP synthase. *Biochemistry* **1995**, *34*, 1635−1645.

(82) Gronenborn, A. M.; Filpula, D. R.; Essig, N. Z.; Achari, A.; Whitlow, M.; Wingfield, P. T.; Clore, G. M. A novel, highly stable fold of the immunoglobulin binding domain of streptococcal protein G. *Science* **1991**, *253*, 657−661.

(83) Poncelet, M.; Huffman, J. L.; Khramtsov, V. V.; Dhimitruka, I.; Driesschaert, B. Synthesis of hydroxyethyl tetrathiatriarylmethyl radicals OX063 and OX071. *RSC Adv.* **2019**, *9*, 35073−35076.

(84) Cunningham, T. F.; McGoff, M. S.; Sengupta, I.; Jaroniec, C. P.; Horne, W. S.; Saxena, S. High-resolution structure of a protein spin-label in a solvent-exposed β-sheet and comparison with DEER spectroscopy. *Biochemistry* **2012**, *51*, 6350−6359.

(85) Singewald, K.; Lawless, M. J.; Saxena, S. Increasing nitroxide lifetime in cells to enable in-cell protein structure and dynamics measurements by electron spin resonance spectroscopy. *J. Magn. Reson.* **2019**, *299*, 21−27.

(86) Saxena, S.; Freed, J. H. Double quantum two-dimensional Fourier transform electron spin resonance: Distance measurements. *Chem. Phys. Lett.* **1996**, *251*, 102−110.

(87) Jeschke, G.; Chechik, V.; Ionita, P.; Godt, A.; Zimmermann, H.; Banham, J.; Timmel, C. R.; Hilger, D.; Jung, H. DeerAnalysis2006—a comprehensive software package for analyzing pulsed ELDOR data. *Appl. Magn. Reson.* **2006**, *30*, 473−498.

(88) Abdullin, D.; Brehm, P.; Fleck, N.; Spicher, S.; Grimme, S.; Schiemann, O. Pulsed EPR Dipolar Spectroscopy on Spin Pairs with one Highly Anisotropic Spin Center: The Low-Spin FeIII Case. *Chem. - Eur. J* **2019**, *25*, 14388−14398.

(89) Decroos, C.; Li, Y.; Soltani, A.; Frapart, Y.; Mansuy, D.; Boucher, J.-L. Oxidative decarboxylation of tris-(p-carboxyltetrathiaaryl)methyl radical EPR probes by peroxidases and related hemeproteins: intermediate formation and characterization of the corresponding cations. *Arch. Biochem. Biophys.* **2010**, *502*, 74−80.

(90) Kuzhelev, A. A.; Trukhin, D. V.; Krumkacheva, O. A.; Strizhakov, R. K.; Rogozhnikova, O. Y.; Troitskaya, T. I.; Fedin, M. V.; Tormyshev, V. M.; Bagryanskaya, E. G. Room-Temperature Electron Spin Relaxation of Triarylmethyl Radicals at the X- and Q-Bands. *J. Phys. Chem. B* **2015**, *119*, 13630−13640.

(91) Shevelev, G. Y.; Krumkacheva, O. A.; Lomzov, A. A.; Kuzhelev, A. A.; Rogozhnikova, O. Y.; Trukhin, D. V.; Troitskaya, T. I.; Tormyshev, V. M.; Fedin, M. V.; Pyshnyi, D. V.; et al. Physiological-temperature distance measurement in nucleic acid using triarylmethyl-based spin labels and pulsed dipolar EPR spectroscopy. *J. Am. Chem. Soc.* **2014**, *136*, 9874−9877.

(92) Giannoulis, A.; Yang, Y.; Gong, Y.-J.; Tan, X.; Feintuch, A.; Carmieli, R.; Bahrenberg, T.; Liu, Y.; Su, X.-C.; Goldfarb, D. DEER distance measurements on trityl/trityl and Gd(iii)/trityl labelled proteins. *Phys. Chem. Chem. Phys.* **2019**, *21*, 10217−10227.

(93) Song, Y.; Liu, Y.; Hemann, C.; Villamena, F. A.; Zweier, J. L. Esterified dendritic TAM radicals with very high stability and enhanced oxygen sensitivity. *J. Org. Chem.* **2013**, *78*, 1371−1376.

(94) Chen, H.; Maryasov, A. G.; Rogozhnikova, O. Y.; Trukhin, D. V.; Tormyshev, V. M.; Bowman, M. K. Electron spin dynamics and spin-lattice relaxation of trityl radicals in frozen solutions. *Phys. Chem. Chem. Phys.* **2016**, *18*, 24954−24965.

(95) Jeschke, G.; Polyhach, Y. Distance measurements on spin-labelled biomacromolecules by pulsed electron paramagnetic resonance. *Phys. Chem. Chem. Phys.* **2007**, *9*, 1895−1910.

(96) Schweiger, A.; Jeschke, G. *Principles of Pulse Electron Paramagnetic Resonance; Illustrated, Reprint.*; Oxford University Press, 2001.

(97) Hagelueken, G.; Ward, R.; Naismith, J. H.; Schiemann, O. MtsslWizard: In Silico Spin-Labeling and Generation of Distance Distributions in PyMOL. *Appl. Magn. Reson.* **2012**, *42*, 377−391.

(98) Bobko, A. A.; Kirilyuk, I. A.; Grigor'ev, I. A.; Zweier, J. L.; Khramtsov, V. V. Reversible reduction of nitroxides to hydroxylamines: roles for ascorbate and glutathione. *Free Radicals Biol. Med.* **2007**, *42*, 404−412.

(99) Sunda, W. G.; Huntsman, S. A. Regulation of cellular manganese and manganese transport rates in the unicellular alga Chlamydomonas 1. *Limnol. Oceanogr.* **1985**, *30*, 71−80.

(100) Widder, P.; Schuck, J.; Summerer, D.; Drescher, M. Combining site-directed spin labeling in vivo and in-cell EPR distance determination. *Phys. Chem. Chem. Phys.* **2020**, *22*, 4875−4879.

(101) Brewer, C. F.; Riehm, J. P. Evidence for possible nonspecific reactions between N-ethylmaleimide and proteins. *Anal. Biochem.* **1967**, *18*, 248−255.

(102) Rhee, S. G.; Chae, H. Z.; Kim, K. Peroxiredoxins: a historical overview and speculative preview of novel mechanisms and emerging concepts in cell signaling. *Free Radicals Biol. Med.* **2005**, *38*, 1543−1552.

(103) Ziegler, D. M. Role of reversible oxidation-reduction of enzyme thiols-disulfides in metabolic regulation. *Annu. Rev. Biochem.* **1985**, *54*, 305−329.

https://doi.org/10.1021/acs.jpcb.1c02371
J. Phys. Chem. B XXXX, XXX, XXX−XXX